Minimal Matchings for dP3 Cluster Variables

Judy Hsin-Hui Chiang[a] Gregg Musiker[a] Son Nguyen[b]

Submitted: May 23, 2025; Accepted: Feb 11, 2026; Published: Jun 5, 2026

Abstract

In previous work [17], Lai and Musiker studied a family of subgraphs of the dP3 brane tiling, called Aztec castles, whose dimer partition functions provide combinatorial formulas for cluster variables resulting from mutations of the quiver associated with the del Pezzo surface dP3. In our paper, we investigate a variant of the dP3 quiver by considering a second alphabet of variables that breaks the symmetries of the relevant recurrences. This deformation is motivated by the theory of cluster algebras with principal coefficients introduced by Fomin and Zelevinsky. Our main result gives an explicit formula extending previously known generating functions for dP3 cluster variables by using Aztec castles and constructing their associated minimal matchings.

Mathematics Subject Classifications: 05C70, 06A07, 13F60

Keywords: Cluster algebras, minimal matchings, del Pezzo 3 lattice

Contents

[a]School of Mathematics, University of Minnesota, Minneapolis, MN, USA (hchiang@umn.edu,musiker@umn.edu)
[b]Department of Mathematics, MIT, Cambridge, MA, USA (sonnvt@mit.edu)

1 Introduction

Upon Fomin and Zelevinsky's pioneering work [7, 8] in cluster algebras for the study of total positivity and dual canonical bases in semisimple Lie groups, a great variety of its applications have been found in combinatorics, tropical geometry [23], Teichmüller theory [9], and representation theory [12]. With the introduction of the Laurent phenomenon, mathematicians ([16, 22, 10]) have been intrigued to study combinatorial interpretations for the cluster variables as perfect matchings of graphs, under suitable weighting schemes. Of particular interest is the situation where the graphs are directly related to the quiver of the cluster algebra, namely when they are subgraphs of the dual of the quiver.

One example of this is [1] where Bousquet-Mélou, Propp, and West introduced a family of graphs known as pinecones and showed the sequence of integers given by the enumeration of perfect matchings of pinecones satisfies the Gale-Robinson recurrence. As a follow-up to this, Jeong, Musiker, and Zhang [11] re-interpreted the weight generating functions of such perfect matchings in terms of framed quivers (see Section 2.5) of cluster theory. See also [25] for a related treatment using the language of T-systems.

The main concern of our paper is the *del Pezzo 3 (dP3) quiver* shown in Figure 1. Denote μ_i a mutation at vertex i. In this paper, we will consider the actions defined in Definition 5:

$$\tau_1 = \mu_1 \circ \mu_2 \circ (12),$$

$$\tau_2 = \mu_3 \circ \mu_4 \circ (34),$$

$$\tau_3 = \mu_5 \circ \mu_6 \circ (56),$$

$$\tau_4 = \mu_1 \circ \mu_4 \circ \mu_1 \circ \mu_5 \circ \mu_1 \circ (145),$$

$$\tau_5 = \mu_2 \circ \mu_3 \circ \mu_2 \circ \mu_6 \circ \mu_2 \circ (236),$$

In [26], Zhang proved an explicit formula for the cluster variables of the dP3 quiver under a sequence of mutations $\tau_1\tau_2\tau_3\tau_1\tau_2\tau_3\ldots$ as perfect matchings of Aztec Dragons. The authors of [18] then found a formula for more general sequences of mutations $\tau_{a_1}\tau_{a_2}\tau_{a_3}\ldots$ for $a_i \in \{1,2,3\}$. Finally, Lai and Musiker [17] found a formula for any sequence of mutations $\tau_{a_1}\tau_{a_2}\tau_{a_3}\ldots$ for $a_i \in \{1,2,3,4,5\}$ as perfect matchings of a certain family of graphs known as Aztec Castles, with Aztec Dragons and the graphs of [18] being special cases. Furthermore, the mutation sequences considered in [17] were general enough to obtain formulas for any cluster variable of the dP3 quiver reachable via a toric mutation sequence, see Section 2.3 for more details.

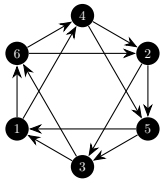

Figure 1: The dP3 quiver

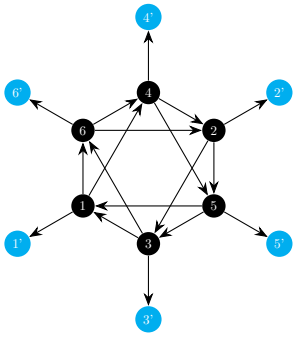

Figure 2: The framed dP3 quiver

Example 1. The cluster variable after the sequence $\tau_1\tau_2\tau_1\tau_3$ is

$$\frac{(x_1x_3+x_2x_4)(x_4x_6+x_3x_5)^2(x_1x_6+x_2x_5)^2}{x_1^2x_2^2x_3^2x_4^2x_6},$$

which is

$$\frac{x_1^2x_2x_3x_4^2x_5x_6^3+x_1^2x_2x_3^2x_4x_5^2x_6^2+x_1^3x_3x_4^2x_6^4+2x_1^3x_3^2x_4x_5x_6^3+\ldots}{x_1^2x_2^2x_3^2x_4^2x_6}.$$

As we will see in Example 6, using prism walks in $\mathbb{Z}^3$, this cluster variable may be indexed as $z_{1,1,1}$, and the corresponding Aztec Castle is $\mathcal{C}_{1,1,1}$ which may be built out of the six-sided contour $(2,-3,2,1,-2,1)$ following the description in Section 2.4.1. Figure 3 shows five perfect matchings of this Aztec Castle. The weight of each of these perfect matchings is a Laurent monomial as we describe in Section 2.4.2 following the construction in [17]. For this example, in the order they are illustrated, they respectively give the monomials

$$\frac{x_5x_6^2}{x_2x_3},\quad \frac{x_5^2x_6}{x_2x_4},\quad \frac{x_1x_6^3}{x_2^2x_3},\quad \frac{2x_1x_5x_6^2}{x_2^2x_4},$$

matching the first four terms in this Laurent expansion. Note that both Figures 3d and 3e give the monomial $\frac{x_1x_5x_6^2}{x_2^2x_4}$, hence the coefficient 2 in the Laurent expansion.

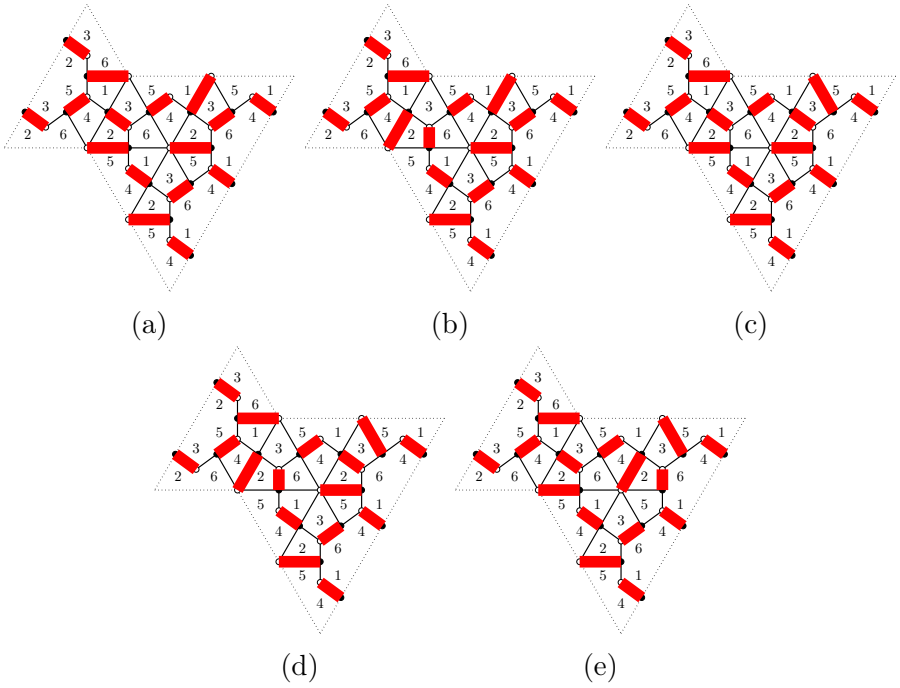

Figure 3: Perfect matchings of the Aztec Castle corresponding to Examples 1 and 2.

In this paper, as analogous to the work in [11] in the case of the Gale-Robinson sequence, we study a framing of the dP3 quiver. We introduce a second set of cluster variables by framing the quiver using new *frozen vertices* in Figure 2. Such a deformation is motivated from Fomin-Zelvinsky's [8] theory of cluster algebras with principal coefficients. A natural question to ask is to find an explicit formula for this new quiver in terms of Aztec Castles.

In the Gale-Robinson sequence case of [11] (resp. the T-systems case of [25]), the Laurent expansions of such cluster variables correspond to perfect matchings of pinecones (resp. crosses-and-wrenches graphs of [22]) and there is a distinguished perfect matching that corresponds to the constant term (relative to the second set of cluster variables) in said expansion. We refer to this as the *minimal matching*, and it can be simply constructed as the perfect matching of the pinecone (resp. crosses-and-wrenches graph) using exclusively horizontal edges (resp. horizontal and diagonal edges [25, Def. 5.2]).

Knowing the minimal matching is enough to recover the cluster variables because every perfect matching can be obtained from the minimal matching by a sequence of face twists (see Section 2.5.2). Recording the faces in this sequence, we get products of y_i's as coefficients of the corresponding monomial. Hence, the question of finding an explicit formula for cluster variables of the framed dP3 quiver amounts to the question of finding the minimal matching of Azter Castles. However, unlike pinecones and crosses-and-wrenches graphs, the construction of minimal matchings of Aztec Castles is more subtle, as we illustrate with our running example.

Example 2. Continuing Example 1, in the framed dP3 quiver, the cluster variable is

$\hat{z}_{1,1,1} =$

$$\frac{x_1^2x_2x_3x_4^2x_5x_6^3 + x_1^2x_2x_3^2x_4x_5^2x_6^2y_2 + x_1^3x_3x_4^2x_6^4y_3 + 2x_1^3x_3^2x_4x_5x_6^3y_2y_3 + \dots}{x_1^2x_2^2x_3^2x_4^2x_6}.$$

In particular, the four monomials in Example 1 appear again, but now with products of y_i's as coefficients

$$\frac{x_5x_6^2}{x_2x_3}, \quad \frac{x_5^2x_6}{x_2x_4}y_2, \quad \frac{x_1x_6^3}{x_2^2x_3}y_3, \quad \frac{2x_1x_5x_6^2}{x_2^2x_4}y_2y_3.$$

This means that the perfect matching in Figure 3a, which corresponds to $\frac{x_5x_6^2}{x_2x_3}$, is the minimal matching. Figure 3b is obtained from Figure 3a by a twist down on a face with label 2, so the corresponding monomial, $\frac{x_5^2x_6}{x_2x_4}y_2$, has coefficient y_2. The perfect matchings in Figures 3c, 3d, and 3e can be obtained analogously by sequences of twist downs from the perfect matching of Figure 3a. Note that the perfect matchings of Figures 3d and 3e involve twist downs at two different faces labeled 2.

Additionally, while not illustrated, the terms in the remainder of the Laurent expansion of this cluster variable for the framed dP3 quiver correspond to additional perfect matchings of this Aztec Castle resulting from applying further twist downs at faces.

Our motivational goal is to provide a direct description of the minimal matching of an Aztec Castle, e.g. the perfect matching of Figure 3a in the case of Example 2. We refer the reader to Appendix A for further examples. We answer this question, thus proving our main result in Section 3. The idea of our construction is as follows. First, we divide the Aztec Castle into four different sectors (see Section 3.1 for details). In each sector, we construct a perfect matching by choosing a periodic set of edges (according to Table 1). By periodic we mean that if an edge between faces i and j is in the perfect matching, then every edge between faces i and j is also in the perfect matching. This gives a universal covering of each sector. Joining together these (four) coverings gives the minimal matching for the Aztec Castle.

Theorem 3 (Theorem 16)**.** *Given an Aztec Castle $\mathcal{C}_{i,j,k}$, the minimal matching whose weight as a perfect matching corresponds to the lowest order term in $\hat{z}_{i,j,k}$ is constructed as described above.*

Contents. The paper is outlined as follows. In Section 2, we review the backgrounds of dP3 quivers, the construction of Aztec castles, and some preliminary results as well as proof techniques from previous work. As just mentioned, our main theorem is the construction of its minimal matching in Section 3. The explicit construction is in Section 3.1 and we also supplement with some examples. We leave our proof of the theorem to Section 4.

2 Background

2.1 Quiver and cluster mutations

A **quiver** Q is a directed finite graph with a set of vertices V and a set of directed edges E connecting them such that there are no loops or 2-cycles. We can relate a **cluster algebra** with **initial seed** $\{x_1, x_2, \ldots, x_n\}$ to Q by associating a cluster variable x_i to every vertex labeled i in Q where $|V| = n$. The **cluster** is the union of the cluster variables at each vertex.

Definition 4. [Quiver Mutation [7]] Mutating at a vertex i in Q is denoted by μ_i and corresponds to the following actions on the quiver:

- For every 2-path through i (e.g. $j \to i \to k$), add an edge from j to k.
- Reverse the directions of the arrows incident to i
- Delete any 2-cycles created from the previous two steps.

When we mutate at a vertex i, the cluster variable at this vertex is updated and all other cluster variables remain unchanged. The action of μ_i on the cluster leads to the following binomial exchange relation:

$$x_i' x_i = \prod_{i \to j \text{ in } Q} x_j^{a_{i\to j}} + \prod_{j \to i \text{ in } Q} x_j^{b_{j\to i}}$$

where x_i' is the new cluster variable at vertex i, $a_{i\to j}$ denotes the number of edges from i to j, and $b_{j\to i}$ denotes the number of edges from j to i.

It was proved in [7] that every cluster variable is a *Laurent polynomial* in

$$\mathbb{Z}[x_1^{\pm 1}, \ldots, x_n^{\pm 1}],$$

i.e.

$$x_m = \frac{P(x_1, \ldots, x_n)}{x_1^{d_1} \ldots x_n^{d_n}}$$

for all m, where $P(x_1, \ldots, x_n) \in \mathbb{Z}[x_1, \ldots, x_n]$.

2.2 del Pezzo 3 quiver and lattice

The focus of this paper is the **del Pezzo 3 (dP3) quiver** illustrated in Figure 1. By unfolding this quiver, we get the infinite unfolded dP3 quiver as shown in Figure 4. Then, taking the dual graph[1] of the unfolded quiver yields its brane tiling in Figure 5, which

[1]For every node of the quiver, we obtain a face of the brane tiling. For every cycle in the quiver we get a vertex of the brane tiling colored black (resp. white) if the cycle is counter-clockwise (resp. clockwise). For every arrow of the quiver $i \to j$, the two faces labeled i and j share a common edge. This edge connects two vertices, and with respect to the direction of the associated arrow, we get a white vertex on the right and a black vertex on the left.

will be referred to as the **dP3 lattice**. This dP3 lattice is an example of a brane tiling, which are doubly periodic, bipartite, planar graphs that arise in string theory [5]. Using the dimer model on such graphs, theoretical physicists can associate an infinite class of supersymmetric quiver gauge theories to a corresponding toric variety (which is a Calabi–Yau 3-fold) as well as this combinatorial model. They appear physically in string theory through the intersections of NS5 and D5-branes which are dual to a configuration of D3-branes probing the singularity of a toric Calabi–Yau threefold. Because of its geometry connection and how the $(3 + 1)$ dimensional supersymmetric gauge field theory lives on the world volume of the D3-brane, it can be represented by the **dP3 quiver**. In this special case of the dP3 lattice, these brane tilings were used by Cottrell-Young [3] as a version of the domino shuffling algorithm.

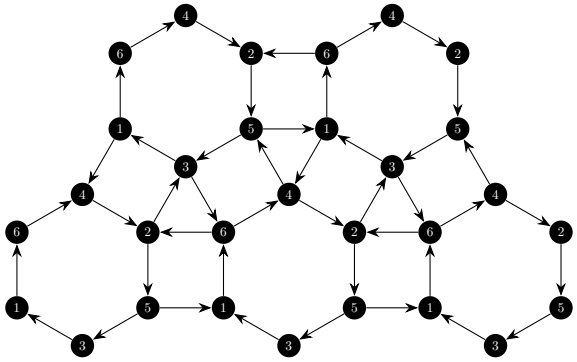

Figure 4: The unfolded dP3 quiver

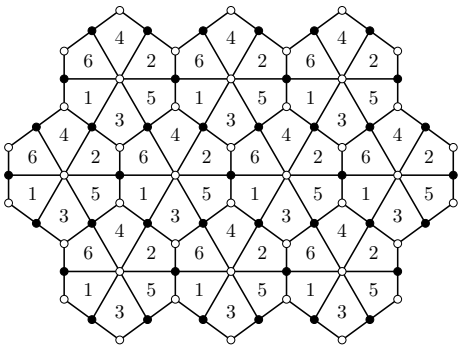

Figure 5: The dP3 lattice

In [17], Lai and Musiker studied sequences of *toric mutations* on the dP3 quiver (see Section 2.3). They found an expression for resulting cluster variables in terms of perfect matchings of *Aztec Castles* (see Section 2.4).

2.3 Toric mutations and prism walk

2.3.1 Toric mutations

A vertex is **toric** if its in-degree and out-degree are both 2. A **toric mutation** is a mutation at a toric vertex. In this paper, we will study the following five actions on the dP3 quiver, which are also the main actions studied in [17].

Definition 5. Define the following actions

$$\tau_1 = \mu_1 \circ \mu_2 \circ (12),$$

$$\tau_2 = \mu_3 \circ \mu_4 \circ (34),$$

$$\tau_3 = \mu_5 \circ \mu_6 \circ (56),$$

$$\tau_4 = \mu_1 \circ \mu_4 \circ \mu_1 \circ \mu_5 \circ \mu_1 \circ (145),$$

$$\tau_5 = \mu_2 \circ \mu_3 \circ \mu_2 \circ \mu_6 \circ \mu_2 \circ (236),$$

where we apply a graph automorphism of Q and permutation to the labeled seed after the sequence of mutations.

One can then check that on the level of quivers and labeled seeds (i.e. ordered clusters), we have the following identities, which are also noted in [17]: For all i, j such that $1 \leqslant i \neq j \leqslant 3$, we have

$$\begin{gathered}
\tau_1(Q) = \tau_2(Q) = \tau_3(Q) = \tau_4(Q) = \tau_5(Q) = Q \\
(\tau_i)^2\{x_1, x_2 \ldots, x_6\} = (\tau_4)^2\{x_1, x_2 \ldots, x_6\} = (\tau_5)^2\{x_1, x_2 \ldots, x_6\} = \{x_1, x_2 \ldots, x_6\} \\
(\tau_i\tau_j)^3\{x_1, x_2 \ldots, x_6\} = \{x_1, x_2 \ldots, x_6\}, \\
\tau_i\tau_4\{x_1, x_2 \ldots, x_6\} = \tau_4\tau_i\{x_1, x_2 \ldots, x_6\}, \\
\tau_i\tau_5\{x_1, x_2 \ldots, x_6\} = \tau_5\tau_i\{x_1, x_2 \ldots, x_6\}.
\end{gathered}$$

2.3.2 Prism walk

We will model the mutations defined in Definition 5 as prism walk on a square triangulated lattice of $\mathbb{Z}^3$, such that a two-dimensional cross-section is illustrated in Figure 6b. We will place the prism so that the coordinates of vertices $1, \ldots, 6$ are $(0, -1, 1), (0, -1, 0), (-1, 0, 0), (-1, 0, 1), (0, 0, 1), (0, 0, 0)$ respectively. The reason is that the cluster variables corresponding to these coordinates, described in Section 2.4, are $x_1, \ldots, x_6$ respectively.

We define the action of μ_i on the prism as follows. First, μ_1 (resp. μ_2) reflects vertex 1 (resp. 2) of the prism about the center of the rectangle formed by vertices $3, 4, 5, 6$. Similarly, μ_3 (resp. μ_4) reflects vertex 3 (resp. 4) of the prism about the center of the rectangle formed by vertices $1, 2, 5, 6$, and μ_5 (resp. μ_6) reflects vertex 5 (resp. 6) of the prism about the center of the rectangle formed by vertices $1, 2, 3, 4$.

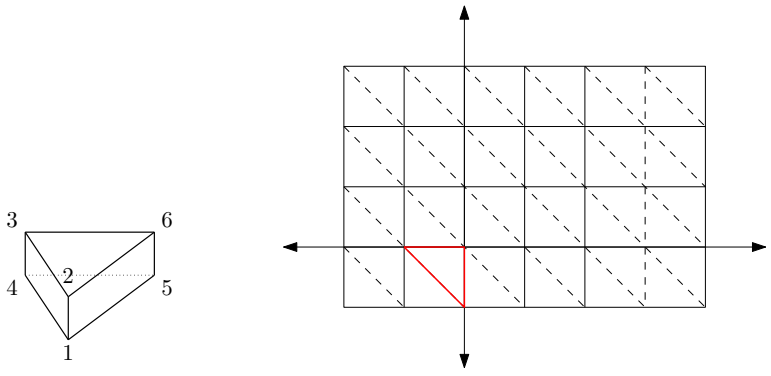

(a) The prism (b) The lattice

Figure 6: Prism and lattice

As a result, the action of τ_1 on the prism can be visualized as in Figure 7. Thus, τ_1 acts on the prism by reflecting the edge 12 about the rectangle formed by vertices $3, 4, 5, 6$. Similarly, τ_2 acts on the prism by reflecting the edge 34 about the rectangle formed by vertices $1, 2, 5, 6$, and τ_3 acts on the prism by reflecting the edge 56 about the rectangle formed by vertices $1, 2, 3, 4$.

Similarly, Figure 8 illustrates the action of τ_4 on the prism. We can see that τ_4 reflects the triangle formed by vertices $1, 4, 5$ about the triangle formed by the other vertices. Similarly, τ_5 reflects the triangle formed by vertices $2, 3, 6$ about the triangle formed by the other vertices.

In summary, the actions of τ_1, τ_2, and τ_3 change the x and y coordinates of the prism while fixing the z coordinate. This is the cross-section illustrated in Figure 6b. The actions of τ_4 and τ_5 change the z coordinate of the prism while fixing the x and y coordinates. One can check that using these five τ-mutations, we can indeed move the original prism to any isometric prism in the $\mathbb{Z}^3$ lattice. Conversely, any sequence of τ-mutations can be modeled as a prism walk in the $\mathbb{Z}^3$ lattice. As a result, we can associate every cluster variable $z_{i,j,k}$ to a point (i, j, k) in $\mathbb{Z}^3$ and vice versa. In the next section, we will also construct an Aztec Castle $\mathcal{C}_{i,j,k}$ for each point (i, j, k). For *nice* Aztec Castles, we can express $z_{i,j,k}$ in terms of perfect matchings of $\mathcal{C}_{i,j,k}$ (see Theorem 10).

Example 6. Recall the sequence $\tau_1\tau_2\tau_1\tau_3$ from Example 1. The positions of the prism

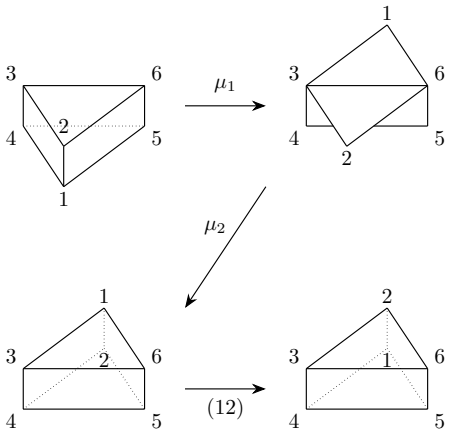

Figure 7: τ_1 action on the prism

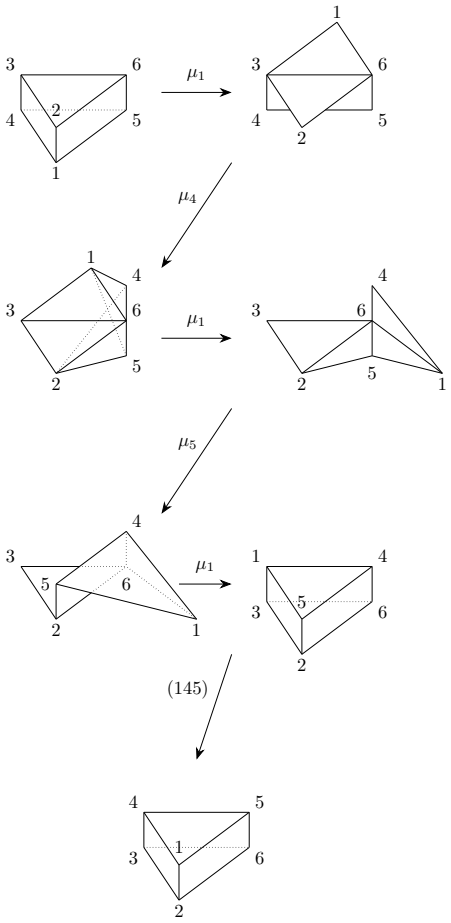

Figure 8: τ_4 action on the prism

after these actions are

$$\{1:(0,-1,1),2:(0,-1,0),3:(-1,0,0),4:(-1,0,1),5:(0,0,1),6:(0,0,0)\}$$
$$\downarrow \tau_1$$
$$\{1:(-1,1,1),2:(-1,1,0),3:(-1,0,0),4:(-1,0,1),5:(0,0,1),6:(0,0,0)\}$$
$$\downarrow \tau_2$$
$$\{1:(-1,1,1),2:(-1,1,0),3:(0,1,0),4:(0,1,1),5:(0,0,1),6:(0,0,0)\}$$
$$\downarrow \tau_1$$
$$\{1:(1,0,1),2:(1,0,0),3:(0,1,0),4:(0,1,1),5:(0,0,1),6:(0,0,0)\}$$
$$\downarrow \tau_3$$
$$\{1:(1,0,1),2:(1,0,0),3:(0,1,0),4:(0,1,1),5:(1,1,1),6:(1,1,0)\}$$

At the end of the sequence, the two new vertices are $5 : (1, 1, 1)$ and $6 : (1, 1, 0)$. As we will see in Theorem 10, the two new cluster variables correspond to the Aztec Castles $\mathcal{C}_{1,1,1}$ and $\mathcal{C}_{1,1,0}$. This matches Example 1.

2.4 Aztec Castles

2.4.1 Construction

In this section, we review the construction of **Aztec Castles** in [17]. In general, the construction of Aztec Castles consists of the following steps.

- *Step 1:* We associate each point $(i, j, k) \in \mathbb{Z}^3$ with a 6-tuple

$$(j + k, -i - j - k, i + k, j + 1 - k, -i - j - 1 + k, i + 1 - k).$$

  We will explain this 6-tuple later in this section.

- *Step 2:* We draw a **(six-sided) contour** $\mathcal{C}(j+k, -i-j-k, i+k, j+1-k, -i-j-1+k, i+1-k)$ on the dP3 lattice in the direction in Figure 9. We start from a vertex in the center of a hexagon and define the unit length to be two "long" edges of the lattice. Note that if an element of the tuple is 0, we simply skip the corresponding side, and if an element is negative, we traverse in the opposite direction.

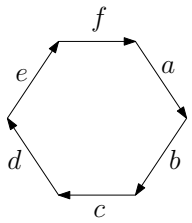

Figure 9: Contour directions

- *Step 3:* We remove every vertex outside the contour and keep only the vertices inside.

- *Step 4:* We remove vertices along the sides as follows. For any side of positive (resp. negative) length, we remove all black (resp. white) vertices along that side. This side corresponds to a single vertex for any side of length zero. If any of the adjacent sides is negative, then this vertex is already removed. If this side is between two sides of length zero, we will also remove this vertex. The only case in which we keep this vertex is when it is between two sides of positive lengths.

- *Step 5:* Finally, we have some "dangling" edges, which are edges in which one of the two incident vertices has degree 1. These are the red edges in Figure 10c. For these edges, we can either keep or remove the two incident vertices. The reason is that when considering perfect matchings of this graph, these edges are always forced to

be in the matching, and they do not contribute to the weight of the matching (which will be defined in Section 2.4.2). For most of this paper, we opt to keep these edges and call the resulting graph $\mathcal{C}_{i,j,k}$.

Figure 10 illustrates the construction of an Aztec Castle starting from the contour $\mathcal{C}(4,-3,0,3,-2,-1)$. The red point in Figure 10a marks the starting point of the contour.

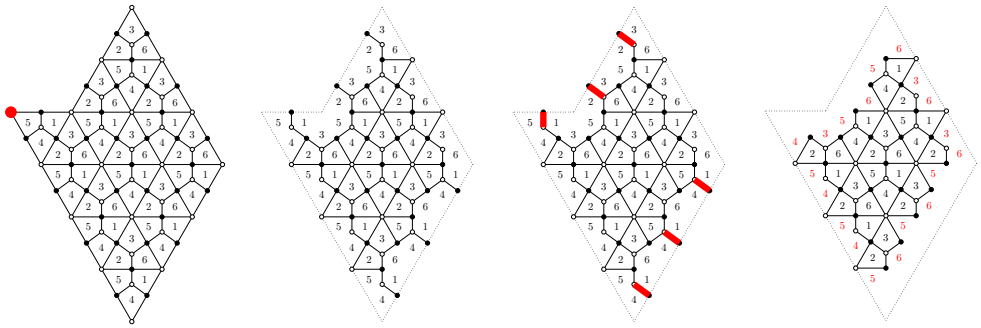

(a) Step 3 (b) Step 4 (c) Step 5: $\mathcal{C}_{i,j,k}$ (d) $\hat{\mathcal{C}}_{i,j,k}$

Figure 10: Aztec Castle construction

Now, we introduce some terminologies that will be used in Section 2.4.2 when discussing the weight of a perfect matching of Aztec Castles. Since the dangling edges do not contribute to the weight, we delete all dangling edges and subsequently all faces that do not have any incident edges left. We define the graph after such deletion $\hat{\mathcal{C}}_{i,j,k}$. Also, we can define *interior* of the graph, denoted as $\mathcal{C}^{\circ}_{i,j,k}$, to be the set of faces that have four edges in $\mathcal{C}_{i,j,k}$. We define the *boundary* of the graph, denoted as $\partial\mathcal{C}_{i,j,k}$, to be the set of faces with fewer than four edges. For example, Figure 10d shows the faces of $\hat{\mathcal{C}}_{i,j,k}$. We mark the numerical labels corresponding to the faces in $\partial\mathcal{C}_{i,j,k}$ in red, and the ones corresponding to the remaining faces in $\mathcal{C}^{\circ}_{i,j,k}$ in black.

We now explain the 6-tuple (a,b,c,d,e,f) in Step 1, as described in Lemma 5.3 of [17]. First of all, for the contour to be closed, we want

$$a+b=d+e \quad \text{and} \quad c+d=f+a.$$

We also want $b+c=e+f$, but this is implied by the above two relations, so we do not include this condition. Finally, since we will work with perfect matchings of this graph, we want the same number of white vertices and black vertices. By counting the number of vertices deleted on each side in step 3 of the construction, Lai and Musiker introduced a third condition which allows for an equal number of black and white vertices:

$$a+b+c+d+e+f=1.$$

One can check that the tuple

$$(a,b,c,d,e,f)=(j+k,-i-j-k,i+k,j+1-k,-i-j-1+k,i+1-k)$$

satisfies all three aforementioned conditions.

Figure 11 shows the possible Aztec Castle shapes when $k \geqslant 1$. There are Aztec Castles from contours that have self-intersections. However, in this paper, we do not consider such Aztec Castles. The reason is apparent from Theorem 10. Hence, in this paper, when we say Aztec Castles, we assume no self-intersections, i.e. we will only consider points outside the yellow region in Figure 11.

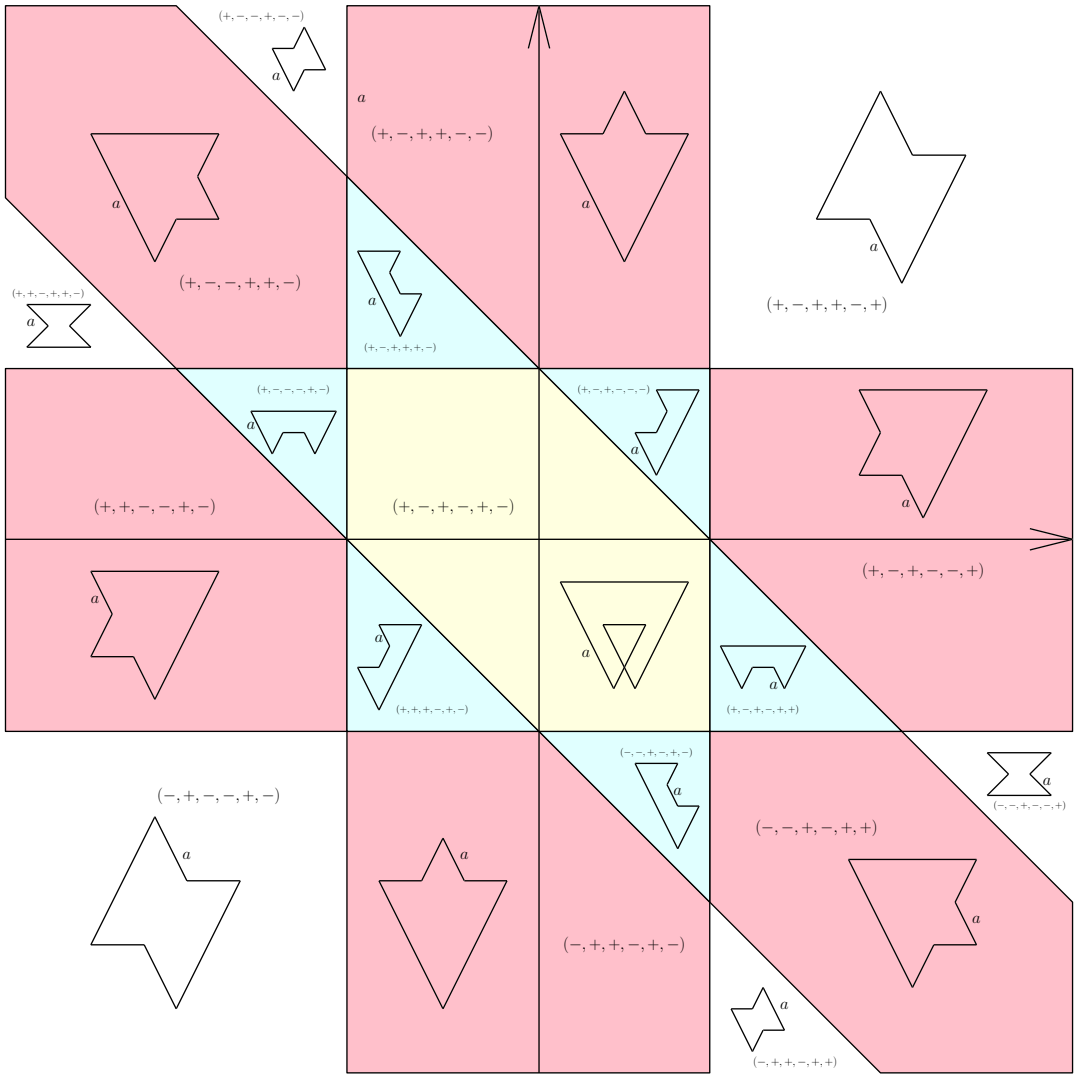

Figure 11: Possible shapes of Aztec Castles when $k \geqslant 1$; the horizontal and vertical axes are i and j, respectively.

As illustrated in Figure 11, as i, j, and k vary, the signs of a, b, c, d, e, and f in the 6-tuple (a, b, c, d, e, f) vary accordingly. We refer to the record of these signs as a **sign pattern**, which we denote as $(s_1, s_2, s_3, s_4, s_5, s_6)$ with $s_i \in \{-, +\}$. For clarity of how the tuples correspond to each region according to the sign patterns, we have the following remarks.

Remark 7. Figure 11 only shows the possible Aztec Castle shapes when $k \geqslant 1$. When $k \leqslant 0$, the sign patterns differ by a cyclic shift of three indices, i.e. $(s_1, s_2, s_3, s_4, s_5, s_6) \to (s_4, s_5, s_6, s_1, s_2, s_3)$. For example, the sign pattern of the top middle pink region when $k \geqslant 1$ is $(+,-,+,+,-,-)$ as in Figure 11. Then, when $k \leqslant 0$, the sign pattern of this region is $(+,-,-,+,-,+)$. Observe that the shapes in the white region actually stay the same under this cyclic shift.

Remark 8. From Figure 11, we have the sign patterns break into orbits under rotations as follows. In the white regions, the sign patterns are $(+,-,+,+,-,+)$, $(-,+,-,-,+,-)$, and their cyclic rotations. In the pink regions, the sign patterns are $(+,+,-,-,+,-)$, $(-,-,+,+,-,+)$, and their cyclic rotations. In the blue regions, the sign patterns are $(+,+,+,-,+,-)$, $(-,-,-,+,-,+)$, and their cyclic rotations. Note that it suffices to discuss only the $k \geqslant 1$ cases since the $k \leqslant 0$ cases will follow from Remark 7. This is because, for each region, a sign pattern will include exactly half of the subregions up to cyclic rotations. For example, in the pink region, three cyclic rotations of $(+,+,-,-,+,-)$ and three cyclic rotations of $(-,-,+,+,-,+)$ each show up as subregions for $k \geqslant 1$ cases and the rest for $k \leqslant 0$. Similar results occur for the blue regions, as well as for the white regions (except there are only three cyclic rotations of each representative in the latter case). Hence, up to cyclic rotation, then it is sufficient to only consider the $k \geqslant 1$ case for our purpose.

Remark 9. By the explicit description of sign patterns given by Remark 8, it follows that for generic non-self-intersecting Aztec Castles, when traversing around the contours, the signs of the sides change exactly four times.

2.4.2 Weight

For every Aztec Castle $\mathcal{C}_{i,j,k}$, we will use the common definition of the weight of a perfect matching m as defined by Speyer in [22]. Following Speyer, let G be a general bipartite planar graph and fix a perfect matching m of G. For a face f which is a $2s$-gon in G, let $E(f)$ denote the edges of G incident to that face, and define

$$\epsilon(f) = \begin{cases} (s-1) - |E(f) \cap m| & \text{if } f \in G^\circ, \\ \left\lceil \frac{E(f)}{2} \right\rceil - |E(f) \cap m| & \text{if } f \in \partial G. \end{cases}$$

where G° denotes the set of interior faces of G and ∂G denotes the set of boundary faces[2]. Let $F(G)$ be the set of all faces of G, including both interior and boundary ones. Then, the weight of m is defined as

$$wt(m) = \prod_{f \in F(G)} x_f^{\epsilon(f)}.$$

[2]In [22], Speyer instead defines $\epsilon(f) = \left\lceil \frac{b-a}{2} \right\rceil$ or $\left\lceil \frac{b-a}{2} \right\rceil - 1$ where a is the number of edges of f that lie in m and b is the number of edges of f not in m. Our definition is equivalent since $a + b = |E(f)| = 2s$ and $a = |E(f) \cap m|$.

Note that each face variable x_f coincides with the cluster variable x_i assigned to the corresponding face f; that is,

$$x_f = x_i \qquad \text{where face } f \text{ is labeled by } i \in \{1, 2, \ldots, 6\} \text{ given the face labeling of } \hat{\mathcal{C}}_{i,j,k}.$$

In our discussion of Aztec Castles, we specialize to the graph $G = \mathcal{C}_{i,j,k}$, and denote by $\hat{\mathcal{C}}_{i,j,k}$ the induced subgraph on the set of faces $F(\mathcal{C}_{i,j,k})$, obtained by deleting the dangling edges in Step 5 (see Figure 10d). Since all faces are 4-gons, the weight formula simplifies to

$$wt(m) = \prod_{f \in \hat{\mathcal{C}}_{i,j,k}} x_f^{(1-|E(f)\cap m|)}.$$

With the weight of each perfect matching defined, we have the following definition of the weight of an Aztec Castle:

$$wt(\mathcal{C}_{i,j,k}) = \sum_{m \text{ is a perfect matching of } \mathcal{C}_{i,j,k}} wt(m).$$

Lai and Musiker proved the following theorem about Aztec Castles.

Theorem 10 ([17] Theorem 5.9)**.** *Let $z_{i,j,k}$ be the cluster variable at point (i, j, k). If the contour $\mathcal{C}(j + k, -i - j - k, i + k, j - k + 1, -i - j + k - 1, i - k + 1)$ defined above, in Step 2 of Section 2.4.1, does not have self-intersections, then*

$$z_{i,j,k} = wt(\mathcal{C}_{i,j,k}).$$

2.5 Framed quiver and minimal matching

2.5.1 Framed quiver

For a quiver Q, the associated **framed quiver** $\hat{Q}$ is a directed graph in which

$$V_{\hat{Q}} = V_Q \ \cup \ \{v_{i+n} \mid v_i \in V_Q\} \quad \text{and} \quad E_{\hat{Q}} = E_Q \ \cup \ \{v_i \to v_{i+n} \mid v_i \in V_Q\}.$$

For instance, the framed quiver of the dP3 quiver in Figure 1 is the quiver in Figure 2. The additional vertices in $\hat{Q}$ are called *frozen vertices*, which means that we never mutate at these vertices. We also associate new cluster variables $\{y_1, \ldots, y_n\}$ to the frozen vertices. Then, every cluster variable for this framed quiver is a Laurent polynomial in $\mathbb{Z}[x_1^{\pm 1}, \ldots, x_n^{\pm 1}, y_1, \ldots, y_n]$, i.e. for all cluster variable $\hat{z}$, one can write

$$\hat{z} = \frac{P(x_1, \ldots, x_n, y_1, \ldots, y_n)}{x_1^{d_1} \ldots x_n^{d_n}},$$

where $P \in \mathbb{Z}[x_1, \ldots, x_n, y_1, \ldots, y_n]$. Following [8, Theorem 3.7, Conjecture 5.4] as well as [4, Theorem 1.7, Proposition 3.1], there is a unique term in this

$$\mathbb{Z}[x_1^{\pm 1}, \ldots, x_n^{\pm 1}, y_1, \ldots, y_n]$$

expansion for $\hat{z}$ with no y_i's occuring as a factor.

Given Theorem 10, the cluster variables $z_{i,j,k}$ are expected to be generating functions (or termed weighted sums) over perfect matchings of the corresponding Aztec Castles $\mathcal{C}_{i,j,k}$. In this case, to account for the extra y_i's, instead of simply taking the weight defined in Section 2.4.2, we also need to introduce the notion of **height** for each perfect matching.

We first adapt the result of Theorem 10 to write

$$\hat{z}_{i,j,k} = \sum_{m \text{ is a perfect matching of } \hat{\mathcal{C}}_{i,j,k}} wt(m)\ y(m)$$

where each $y(m)$ is a monomial in $\{y_1, y_2, \ldots, y_6\}$ and there is a unique term with $y(m) = 1$. We let m_0 denote the unique perfect matching corresponding to $y(m_0) = 1$ in this Laurent expansion. We may refer to the exponent vectors of the $y(m)$'s as **height functions** as we now describe.

Historically, height functions are first defined in Elkies, Larsen, Kuperberg, and Propp [6], inspired by earlier work enumerating tilings including work of Conway-Lagarias [2] and Thurston [24]. Musiker and Schiffler [20] originated the use of height functions in cluster algebras. They ([20, Remark 5.3]) proved that the minimal matching of a so-called snake graph is the same as the minimal element of the associated twist down lattice studied by Propp in [21]. Their argument can be adapted to the case of Aztec Castles instead of snake graphs. (Our proof uses [21, Theorem 2], which we include below as 12.) See also [19] for a more recent treatment for general bipartite plane graphs. Note that the notion of height functions is also well-studied in the dimer model and statistical mechanics [15, 14, 13]. As mentioned in [19], there is a nontrivial translation between the two notions. But here we only focus on the use of height function in the context of cluster algebras, and will exclusively focus on the case where our graph is an Aztec Castle $\hat{\mathcal{C}}_{i,j,k}$.

Definition 11. Given a choice of a minimal matching m_0 of $\hat{\mathcal{C}}_{i,j,k}$, we define the **height** of m_0 to be the zero vector, and the height of any other perfect matching m of $\hat{\mathcal{C}}_{i,j,k}$ is defined to be the vector $\mathsf{ht}(m) = (d_1, d_2, \ldots, d_6) \in \mathbb{N}^6$ constructed as follows: Superimpose m with m_0 to create one or more closed loops $\{C_1, C_2, \ldots, C_s\}$. With respect to the face labeling given to $\hat{\mathcal{C}}_{i,j,k}$, we let d_i denote the number of faces f labeled as i that are enclosed by loop(s) $C_1, C_2, \ldots, C_s$, taken possibly with multiplicity. We then let $y(m) = \prod_{i=1}^{6} y_i^{d_i}$.

A priori, there could be multiple choices for m_0, but as we see in Theorem 12, the minimal matching can be defined uniquely based on the twist down lattice. In particular, as suggested by Definition 11, our main question is: what is the *correct minimal matching* of Aztec Castles? The next section gives a criterion for finding the minimal matching.

2.5.2 Twist down lattice of perfect matchings

Given graph $\mathcal{C}_{i,j,k}$ (defined as an Aztec Castle with the dangling edges removed), we may temporarily forget the labeling of faces in $\partial\mathcal{C}_{i,j,k}$ and consider the exterior to be a single unbounded face which we denote as f^*. A **face twist** on a perfect matching is the

operation of removing the edges that form an alternating cycle of a face and inserting the complementary edges. We call a face **twistable** if a face twist can be applied to it. In other words, a $2s$-gon face is twistable if it has s edges in the perfect matching, and a face twist on this face will replace the s edges by the other s edges.

We say a twistable face of the Aztec Castle is **positive** (resp. **negative**) if the edges contained in a perfect matching, when directed from black vertices to white vertices, circle the face in a counterclockwise (resp. clockwise) direction. A **twist down** is a face twist that converts a positive face to a negative face, and a **twist up** is a face twist that converts a negative face to a positive face. This face twist operation gives a distributive lattice on the set of perfect matchings of an Aztec Castle.

Theorem 12 ([21, Theorem 2])**.** *Let $\mathcal{M}$ be the (non-empty) set of perfect matchings of an Aztec Castle $\mathcal{C}_{i,j,k}$. If we say that one perfect matching M covers another perfect matching N exactly when N is obtained from M by twisting down at a face other than f^*, then the covering relation makes $\mathcal{M}$ into a distributive lattice.*

Figure 12 gives an example of Theorem 12. Furthermore, the unique minimal element of this lattice is the unique perfect matching in which no twisting down at a face other than f^* is possible. In other words, every possible face twist at a face other than f^* is at a negative face. This yields a compact description of the bottom element of the lattice, $\mathcal{M}$, as we summarize in the following corollary.

Corollary 13. *If a perfect matching of an Aztec Castle has no positive twistable face (except the unbounded face), then it is the minimal matching.*

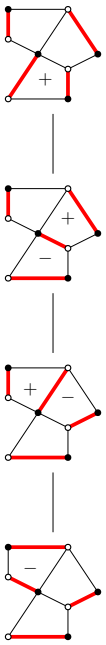

Figure 12: The twist down lattice of an Aztec Castle

3 Minimal matching of Aztec Castles

3.1 Construction

In this section, we will give the construction of the minimal matching, which will be proved later in Section 4. Specifically, we will give the construction for generic cases when none of the sides is 0. When one or more sides equal 0, we give them arbitrary signs. The construction has two main steps.

- *Step 1: Dividing the Castle into sectors.* We traverse along the sides of the contour in a clockwise direction. At each corner, we perform one of the following actions:
  - If we move from a positive side to a positive side, draw a straight line in the direction of the second side.
  - If we move from a negative side to a negative side, draw a straight line in the direction of the first side.
  - If we move from a negative side to a positive side, draw a staircase diagonally, with the first step lying on the positive side.
  - If we move from a positive side to a negative side, no action is required.

  By Remark 9, we move from a negative side to a positive side exactly twice and move between two sides with the same sign exactly twice. Hence, there are exactly two straight lines and two staircases.

  Furthermore, while it is not immediate from the construction, these two straight lines and two staircases intersect at two points (one per pair of line and staircase), and the two points can be connected by a straight line on the lattice. We connect these two points by that straight line, and we call this line the **zero line**. This line is parallel to two opposing sides of the contour (see Remark 15). We will show the existence of this zero line in Section 3.2.

  After this step, the Castle is divided into four sectors, two of them are each incident to one side of the contour while the other two are each incident to two sides.

- *Step 2: Covering each sector according to the side.* We will use a universal covering for each sector, and the covering is determined by the side of the contour that the sector is incident to as in Table 1. Here, for example, by "$1-4$" we mean the edge between faces 1 and 4.

Figure 13 shows an example of this construction. The contour is $\mathcal{C}(5,-9,6,2,-6,3)$, giving the Castle $\mathcal{C}_{4,3,2}$. In Figure 13a, from side a to b, and from side d to e, we move from positive sides to negative sides, so we do nothing. From side b to c, and from side e to f, we move from negative sides to positive sides, so we draw staircases (colored purple) with the first steps lying on the positive sides c and f. From side c to d, and from side f to a, we move from positive sides to positive sides, so we draw straight lines (colored red) in the direction of sides a and d. Furthermore, the two straight lines and staircases meet

Side	Positive	Negative
a	$1-4, 2-5, 3-6$	$1-5, 2-4, 3-6$
b	$1-4, 2-6, 3-5$	$1-4, 2-5, 3-6$
c	$1-3, 2-6, 4-5$	$1-4, 2-6, 3-5$
d	$1-6, 2-3, 4-5$	$1-3, 2-6, 4-5$
e	$1-5, 2-3, 4-6$	$1-6, 2-3, 4-5$
f	$1-5, 2-4, 3-6$	$1-5, 2-3, 4-6$

Table 1: Universal covering for each case

at two points that can be connected by another straight blue line. (In Section 3.2, we will call the blue line the zero line and show its existence). Finally, in Figure 13b, we cover each sector according to Table 1. We refer the readers to Appendix A for more examples.

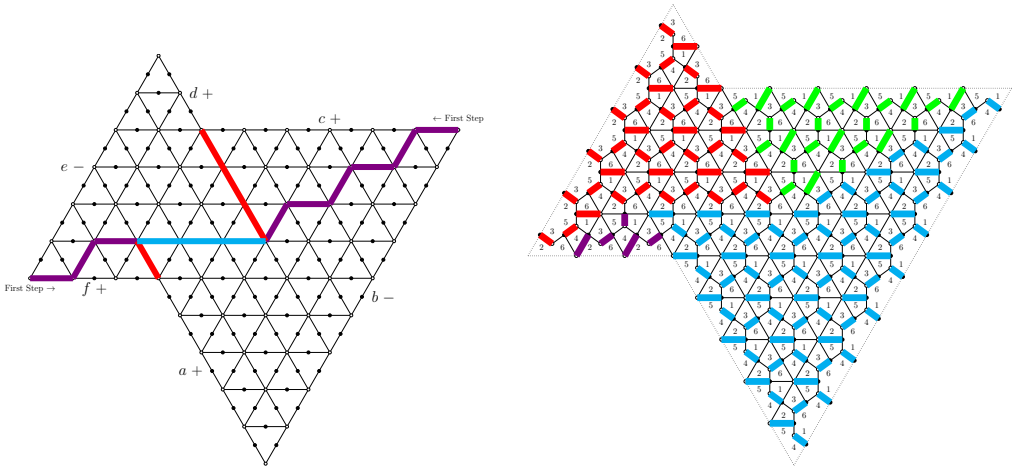

(a) Four sectors (b) Minimal matching

Figure 13: Four sectors and minimal matching of Aztec Castle $\mathcal{C}_{4,3,2}$

Note that in Table 1, the matching when one side is positive is the same as when the next side is negative. This is because in step 1 when moving from a positive side to a negative side, we do nothing, so these two sides are incident to the same sector. Thus, they should have the same universal covering.

Also when two consecutive sides have the same sign, their universal covering has one edge in common. We will see that this leads to a "smooth transition" between the two corresponding sectors. As a result, there will be no twistable face along the straight line dividing the two sectors. The twistable faces do not come from the interior of each sector either. Therefore, they only come from the two staircases and the zero line.

Remark 14. There seems to be a small ambiguity in step 2 above for the covering on the zero line as we may have the choice of which covering to use. However, depending on the parity of the staircases' length, there is a unique covering for this line.

Remark 15. In step 1 of the construction, one can see that the sign pattern of the contour determines the direction of the staircases, the straight lines, and the zero line. Recall from Remark 7 that the sign patterns are $(+,-,\hat{+},+,-,\hat{+})$, $(\hat{-},+,-,\hat{-},+,-)$, $(\hat{+},+,-,\hat{-},+,-)$, $(-,\hat{-},+,+,\hat{-},+)$, $(\hat{+},+,+,\hat{-},+,-)$, and $(-,-,\hat{-},+,-,\hat{+})$. Here, the (opposing) sides with the red signs[3] are those parallel to the zero line. For example, if the sign pattern is $(+,-,\hat{+},+,-,\hat{+})$, then the zero line is parallel to side c and f. On the other hand, if the sign pattern is $(\hat{-},+,-,\hat{-},+,-)$, the zero line is parallel to side a and d.

Theorem 16. *The construction above gives a valid perfect matching, and it is the minimal matching for Aztec Castles.*

3.2 The zero line

In this section, we prove the existence of the zero line. The regions discussed in the following subsections are taken from Figure 11.

3.2.1 White regions

Recall from Remark 8 that in the white regions, the sign patterns are either

$$(+,-,\hat{+},+,-,\hat{+}),(\hat{-},+,-,\hat{-},+,-), \text{ or their cyclic rotations.}$$

Recall also that the sides with the red signs are those parallel to the zero line. For our convenience, let **Region 1** be the top right white region in Figure 11, where $k \geqslant 1$ and $k-1 \leqslant i,j$. Likewise, let **Region 1'** be the top middle region in Figure 11, where $k \geqslant 1$, $k-1 \leqslant i+j$, and $i \leqslant -k$. Note that by Remark 8, the discussion of these 2 cases is sufficient.

Region 1. This region has sign pattern $(+,-,\hat{+},+,-,\hat{+})$, so the zero line is parallel to sides c and f. Figure 14 shows the calculations for this region. Side a has length $j+k$ while side b has length $i+j+k$, so the difference in lengths between sides a and b is $|i| = i$. Side c has length $i+k$, so the height of the staircase is $\left\lfloor \frac{|i+k|}{2} \right\rfloor = \left\lfloor \frac{i+k}{2} \right\rfloor$. Side f has length $i+1-k$, so the height of the staircase is $\left\lfloor \frac{|i+1-k|}{2} \right\rfloor = \left\lfloor \frac{i+1-k}{2} \right\rfloor$. It remains to show that $\left\lfloor \frac{i+k}{2} \right\rfloor + \left\lfloor \frac{i+1-k}{2} \right\rfloor = i$, which is straightforward. If $i-k = 2\ell$, then

$$\left\lfloor \frac{i+k}{2} \right\rfloor + \left\lfloor \frac{i+1-k}{2} \right\rfloor = k+\ell+\ell = k+2\ell = i.$$

If $i-k = 2\ell+1$, then

$$\left\lfloor \frac{i+k}{2} \right\rfloor + \left\lfloor \frac{i+1-k}{2} \right\rfloor = k+\ell+\ell+1 = k+2\ell+1 = i.$$

[3]and hats in case of reading this in grayscale

The arguments for other shapes whose sign patterns are cyclic rotations of

$$(+,-,+,+,-,+)$$

are analogous, and they come down to checking the following three identities:

$$\left\lfloor \frac{i+k}{2} \right\rfloor + \left\lfloor \frac{i+1-k}{2} \right\rfloor = i,$$
$$\left\lfloor \frac{j+k}{2} \right\rfloor + \left\lfloor \frac{j+1-k}{2} \right\rfloor = j,$$
$$\left\lfloor \frac{-i-j-k}{2} \right\rfloor + \left\lfloor \frac{-i-j-1+k}{2} \right\rfloor = -i-j-1.$$

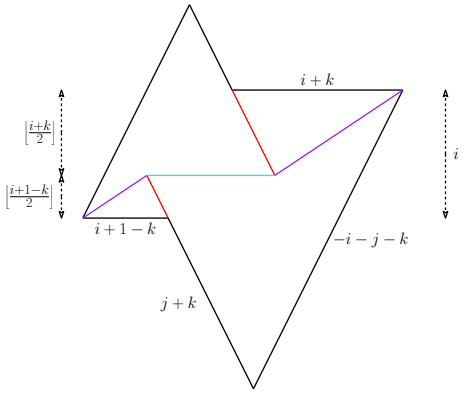

Figure 14: Region 1 zero line

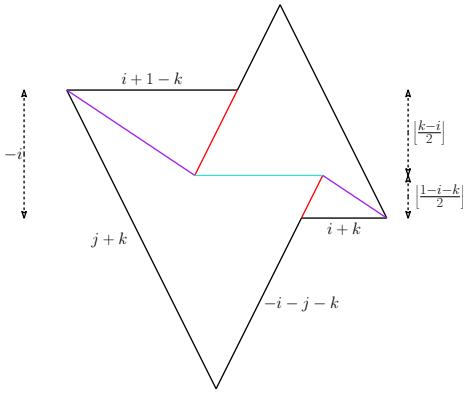

Figure 15: Region 1' zero line

Region 1'. This region has sign pattern $(+,-,\hat{-},+,-,\hat{-})$, so the zero line is parallel to sides c and f. Figure 15 shows the calculations for this region. The difference in lengths between sides f and c is $|i| = -i$. Side c has length $|i+k|$, but the first step of the staircase is on side d, so the height of the staircase is $\left\lfloor \frac{|i+k|+1}{2} \right\rfloor = \left\lfloor \frac{1-i-k}{2} \right\rfloor$. Side f has length $|i+1-k|$, so the height of the staircase is $\left\lfloor \frac{|i+1-k|+1}{2} \right\rfloor = \left\lfloor \frac{k-i}{2} \right\rfloor$. It remains to show that $\left\lfloor \frac{1-i-k}{2} \right\rfloor + \left\lfloor \frac{k-i}{2} \right\rfloor = -i$, which is also straightforward.

The arguments for other shapes whose sign patterns are cyclic rotations of

$$(-,+,-,-,+,-)$$

are analogous, and they come down to checking the following three identities:

$$\left\lfloor \frac{1-i-k}{2} \right\rfloor + \left\lfloor \frac{k-i}{2} \right\rfloor = -i,$$
$$\left\lfloor \frac{1-j-k}{2} \right\rfloor + \left\lfloor \frac{k-j}{2} \right\rfloor = -j,$$
$$\left\lfloor \frac{i+j+k+1}{2} \right\rfloor + \left\lfloor \frac{i+j-k+2}{2} \right\rfloor = i+j+1.$$

3.2.2 Pink regions

In the pink regions, the sign patterns are $(\hat{+}, +, -, \hat{-}, +, -)$, $(-, \hat{-}, +, +, \hat{-}, +)$, and their cyclic rotations. Let **Region 2** be the top middle pink region in Figure 11, where $k \geqslant 1$ and $-k \leqslant i \leqslant k-1 \leqslant j, i+j$. Also, let **Region 2'** be the top left pink region in Figure 11, where $k \geqslant 1$ and $i \leqslant -k \leqslant i+j \leqslant k-1 \leqslant j$. Again, by Remark 8, the discussion of these 2 cases is sufficient.

Region 2. This region has sign pattern $(+, -, \hat{+}, +, -, \hat{-})$, so the zero line is parallel to sides c and f. Figure 16 shows the calculations for this region. The calculations are almost the same as in Region 1. The height of the staircases in this case are $\left\lfloor \frac{|i+k|}{2} \right\rfloor = \left\lfloor \frac{i+k}{2} \right\rfloor$ and $\left\lfloor \frac{|k-1-i|+1}{2} \right\rfloor = \left\lfloor \frac{k-i}{2} \right\rfloor$. We need to check $\left\lfloor \frac{i+k}{2} \right\rfloor - \left\lfloor \frac{k-i}{2} \right\rfloor = i$. This is also straightforward.

Similar to the white regions, the arguments for other shapes whose sign patterns are cyclic rotations of $(+, +, -, -, +, -)$ comes down to checking analogous identities. This is left to the readers.

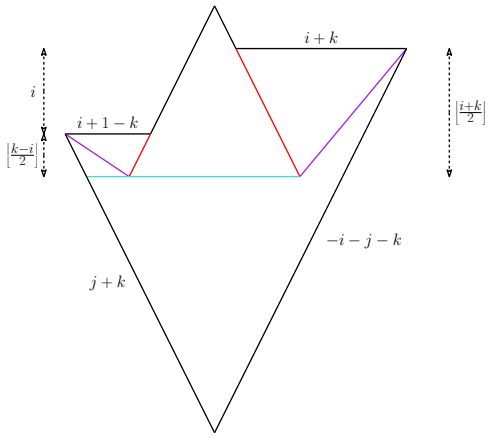

Figure 16: Region 2 zero line

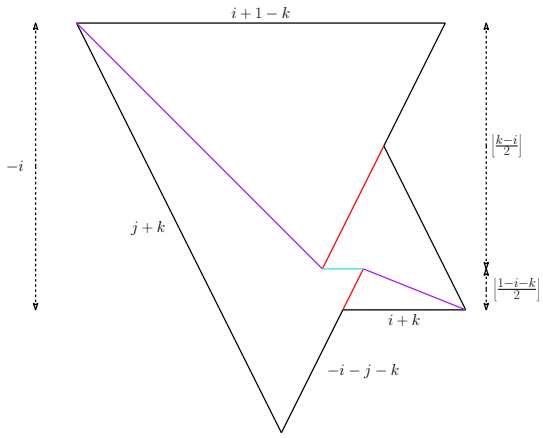

Figure 17: Region 2' zero line

Region 2'. This region has sign pattern $(+, -, \hat{-}, +, +, \hat{-})$, so the zero line is parallel to sides c and f. Figure 17 shows the calculations for this region. Observe that the calculations for this region are exactly the same as for Region 1' above. Hence, the argument for this case is the same as in Section 3.2.1.

3.2.3 Blue regions

Lastly, in the blue regions, the sign patterns are

$$(\hat{+},+,+,\hat{-},+,-), \text{and} (-,-,\hat{-},+,-,\hat{+}), \text{and their cyclic rotations.}$$

Let **Region 3** be the blue region in the first quadrant in Figure 11, where $k \geqslant 1$ and $i, j \leqslant k-1 \leqslant i+j$. Likewise, let **Region 3'** be the top blue region in the second quadrant in Figure 11, where $k \geqslant 1$, $i+j \leqslant k-1 \leqslant j$, and $i \geqslant -k$. It suffices to discuss these 2 cases by Remark 8.

Region 3. This region has sign pattern $(+,-,\hat{+},+,+,\hat{-})$, so the zero line is parallel to sides c and f. Figure 18 shows the calculations for this region. Observe that the calculations for this region are exactly the same as for Region 2 above. Hence, the argument is the same as in Section 3.2.2.

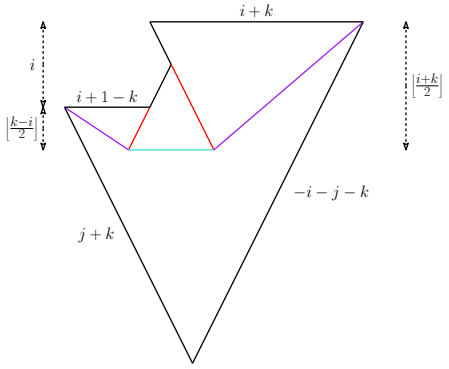

Figure 18: Region 3 zero line

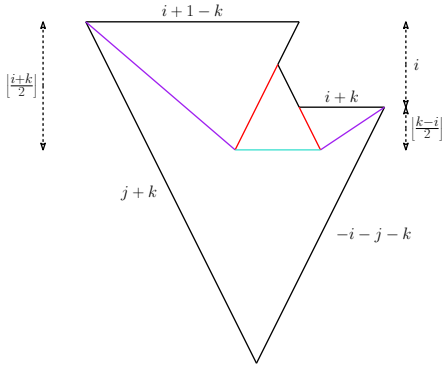

Figure 19: Region 3' zero line

Region 3'. This region has sign pattern $(+,-,\hat{+},-,-,\hat{-})$, so the zero line is parallel to sides c and f. Figure 19 shows the calculations for this region. Observe that the calculations for this region are exactly the same as for Region 3 above. Hence, the argument is also the same as in Section 3.2.2.

4 Proof of Theorem 16

In this section, we first present four lemmas that will be used in proving Theorem 16, and then the proof of Theorem 16.

Lemma 17. *In the interior of each sector, there is no twistable face, and every vertex is covered exactly once.*

Proof. By examining the universal coverings in Table 1, each face in the interior of a sector is incident to exactly one edge of the perfect matching. Figure 13 (b) shows four of the six cases, and the remaining two follow by 60-degree rotational symmetry of these diagrams. The periodic perfect matching thus covers every vertex exactly once. Note that the result of this lemma is independent from the face labeling. □

Lemma 18. *Along the straight line borders, there is no twistable face, and every vertex is covered exactly once.*

Proof. Recall from the construction that there are two scenarios that create a straight line border:

1. we move from a positive side to a positive side, and draw a straight line in the direction of the second side; or
2. we move from a negative side to a negative side, and draw a straight line in the direction of the first side.

Let us show the argument for the first case. The second case follows analogously. In the first case, the matching along the straight line border is as follows:

- The black vertices are covered by the covering in the first side's sector.
- The white vertices are covered by the covering in the second side's sector.
- No edge along the border is covered, and hence there is no twistable face.

Figure 20 shows an example when we move from a positive side a to a positive side b, the straight line is in the direction of side b. The black vertices on the border are covered by the edges $1-4$ in side a's sector. The white vertices on the border are covered by the edges $3-5$ in side b's sector. There is no edges covered along the border, and there is no twistable face. We encourage the readers to check this observation for other pairs of consecutive positive sides.

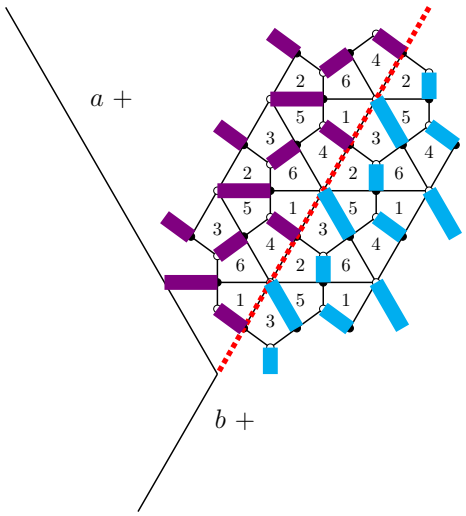

Figure 20: The straight line border (colored red) between positive a and positive b

□

Lemma 19. *Along the staircase borders, all twistable faces are negative, and every vertex is covered exactly once.*

Proof. Recall from the construction that we draw a staircase border when we move from a negative side to a positive side, with the first step lying on the positive side. We call a step on the staircase a *base step* (resp. *side step*) if it is parallel to the positive (resp. negative) side. There are two white vertices and one black vertex on each side step. We call a white vertex on a side step a *white concave-up vertex* (colored red in Figure 21b) if the arrow from it to the black vertex on the same step points in the negative direction of the negative side. We call the other white vertex the *white concave-down vertex* (colored blue in Figure 21b). The matching along the staircase border is as follows:

- On the base steps, the black vertices are covered by the covering in the positive side's sector.
- On the side steps, the white concave-up vertices are covered by the covering in the negative side's sector; and
- the black vertices and the white concave-down vertices are matched following the positive side's sector. The faces containing these edges on the negative side's sector are the negative twistable faces.

Figure 21a shows an example when we move from a negative side b to a positive side c. The black vertices on the base steps are covered by the edges $2-6$ in side c's sector. The white concave-up vertices on the side steps are covered by the edges $2-5$ in side b's sector. The remaining vertices on the side steps are matched by the edges $1-3$. The faces 3 containing these edges on side b's sector are the negative twistable faces. We encourage the readers to check this observation for other pairs of consecutive positive sides.

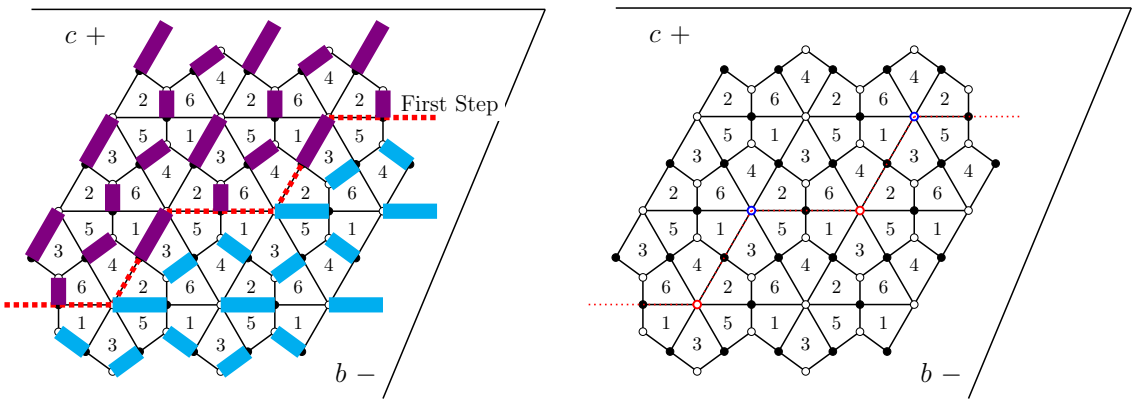

(a) The matching (b) White concave up and down vertices

Figure 21: The staircase border between $b \leqslant 0$ and $c \geqslant 0$

□

Lemma 20. *Along the zero line, all twistable faces are negative, and every vertex is covered exactly once.*

Proof. Similar to Section 3.2, we only need to show the proof for three representative regions:

1. $k \geqslant 1$ and $k - 1 \leqslant i, j$;
2. $k \geqslant 1$ and $-k \leqslant i \leqslant k - 1 \leqslant j, i + j$; and
3. $k \geqslant 1$ and $i, j \leqslant k - 1 \leqslant i + j$.

Note that in all three regions, the two sectors incident to the zero line are incident to a negative side b and a negative side e.

In Region 1, as shown in Section 3.2, the two staircases have lengths of different parity and base steps on parallel sides (c and f), so one of them ends with a side step and the other end with a base step.

By the matching rule along the staircase borders in Lemma 19, of the two endpoints of the zero line, only one is covered. Thus, there are an even number of uncovered vertices on the zero line. If the covered endpoint is covered by the covering of side b (resp. side e), then we can cover the rest of the zero line by the same covering as in Figure 22a (resp. Figure 22b). We refer the readers to Figure 23 and 24 for examples of these coverings. In both cases, the twistable faces containing these edges on the zero line are negative.

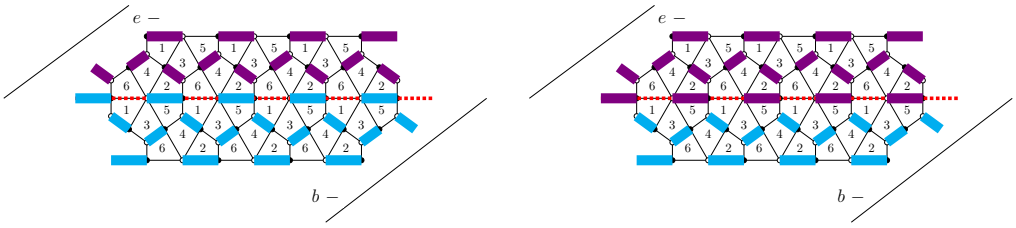

(a) Zero line's matching follows negative b

(b) Zero line's matching follows negative e

Figure 22: The zero line border between negative b and negative e

In Regions 2 and 3, the two staircases have lengths of the same parity but base steps on non-parallel sides (c and a), so the same is true: one of them ends with a side step and the other ends with a base step. Thus, the arguments follow analogously. We refer the readers to Figure 25 and 26 for examples of the coverings. □

Proof of Theorem 16. Recall from Theorem 12 that the minimal matching in the twist down lattice is the one with no positive twistable face except the exterior unbounded face f^*. Lemma 17 implies that there is no twistable face in the interior of each sector, and Lemma 18 there is no twistable face along the straight-line borders. Hence any twistable face is either along the staircase borders or the zero line. Together, Lemmas 19 and 20 then state that any twistable face is negative. As shown in these four lemmas, the proposed construction gives a valid perfect matching in which every vertex is covered exactly once. Theorem 16 then follows from Corollary 13. □

Acknowledgements

This project was partially supported by the RTG grant NSF/DMS-1745638 and the FRG grant NSF/DMS-1854162. It was supervised as part of the University of Minnesota School of Mathematics Summer 2022 REU program. The authors would like to thank Carolyn Stephen and Sylvester Zhang for their continuous support throughout the project. We would also like to thank David Speyer for helpful discussions.

References

[1] Mireille Bousquet-Mélou, James Propp, and Julian West. Perfect matchings for the three-term Gale-Robinson sequences. *Electronic Journal of Combinatorics*, 16(1):#R125, 37, 2009. doi:10.37236/214.

[2] J. H. Conway and J. C. Lagarias. Tiling with polyominoes and combinatorial group theory. *Journal of Combinatorial Theory. Series A*, 53(2): 183–208, 1990. doi:10.1016/0097-3165(90)90057-4.

[3] Cyndie Cottrell and Benjamin Young. Domino shuffling for the Del Pezzo 3 lattice. arXiv:1011.0045, 2010.

[4] Harm Derksen, Jerzy Weyman, and Andrei Zelevinsky. Quivers with potentials and their representations II: applications to cluster algebras. *Journal of the American Mathematical Society*, 23(3): 749–790, 2010. doi:10.1090/S0894-0347-10-00662-4.

[5] Bo Feng, Yang-Hui He, Kristian D Kennaway, and Cumrun Vafa. Dimer Models from Mirror Symmetry and Quivering Amoebae. *Advances in Theoretical and Mathematical Physics*, 12(3): 489–545, 2008. doi:10.4310/atmp.2008.v12.n3.a2.

[6] Noam Elkies, Greg Kuperberg, Michael Larsen, and James Propp. Alternating-sign matrices and domino tilings. II. *Journal of Algebraic Combinatorics. An International Journal*, 1(3): 219-234, 1992.

[7] Sergey Fomin and Andrei Zelevinsky. Cluster algebras I: Foundations. *Journal of the American Mathematical Society*, 15: 497–529, 2001. doi:10.1090/S0894-0347-01-00385-X.

[8] Sergey Fomin and Andrei Zelevinsky. Cluster algebras IV: Coefficients. *Compositio Mathematica*, 143(1): 112—164, 2007. doi:10.1112/S0010437X06002521.

[9] Vladimir Fock and Alexander Goncharov. Moduli spaces of local systems and higher Teichmüller theory. *Publications Mathématiques. Institut de Hautes Études Scientifiques*, 103:1–211, 2006. doi:10.1007/s10240-006-0039-4.

[10] Alexander B. Goncharov and Richard Kenyon. Dimers and cluster integrable systems. *Annales Scientifiques de l'École Normale Supérieure. Quatrième Série*, 46(5): 747–813, 2013. doi:10.24033/asens.2201.

[11] In-Jee Jeong, Gregg Musiker, and Sicong Zhang. Gale-Robinson sequences and brane tilings. *25th International Conference on Formal Power Series and Algebraic Com-*

binatorics (FPSAC 2013), volume AS of Discrete Math. Theor. Comput. Sci. Proc.: 707—718. Assoc. Discrete Math. Theor. Comput. Sci., Nancy, 2013.

[12] Bernhard Keller. Cluster algebras and cluster categories. *Bulletin of the Iranian Mathematical Society*, 37(2): 187–234, 2011.

[13] Richard Kenyon. Local statistics of lattice dimers. *Annales de l'IHP Probabilités et statistiques*. 33(5), 591-618, 1997.

[14] Richard Kenyon. An introduction to the dimer model. *School and Conference on Probability Theory, ICTP Lect. Notes Series*, 17: 267–304. Abdus Salam International Centre for Theoretical Physics, 2009.

[15] Richard Kenyon, Andrei Okounkov, and Scott Sheffield. Dimers and amoebae. *Annals of Mathematics*, 163(3): 1019–1056, 2006.

[16] Eric H. Kuo. Applications of graphical condensation for enumerating matchings and tilings. *Theoretical Computer Science*, 319(1-3), 29-57, 2004.

[17] Tri Lai and Gregg Musiker. Beyond Aztec Castles: Toric Cascades in the dP3 Quiver. *Communications in Mathematical Physics*, 356(3): 823–881, 2017. doi:10.1007/s00220-017-2993-8.

[18] Megan Leoni, Gregg Musiker, Seth Neel, and Paxton Turner. Aztec castles and the dP3 quiver. *Journal of Physics. A. Mathematical and Theoretical*, 47(47): 474011, 32, 2014. doi:10.1088/1751-8113/47/47/474011.

[19] Karola Mészáros, Gregg Musiker, Melissa Sherman-Bennett, and AlexV idinas. Dimer face polynomials in Knot Theory and Cluster Algebras. arXiv:2408.11156, 2024.

[20] Gregg Musiker and Ralf Schiffler. Cluster expansion formulas and perfect matchings. *Journal of Algebraic Combinatorics*, 32: 187–209, 2010. doi:10.1007/s10801-009-0210-3.

[21] James Propp. Lattice structre for orientation of graphs. *Electronic Journal of Combinatorics*, 32:#P4.26, 2025. doi:10.37236/9474

[22] David E. Speyer. Perfect matchings and the octahedron recurrence. *Journal of Algebraic Combinatorics*, 25(3): 309–348, 2007. doi:10.1007/s10801-006-0039-y.

[23] David E. Speyer and Lauren Williams. The tropical totally positive Grassmannian. *Journal of Algebraic Combinatorics*, 22: 189–210, 2005. doi:10.1007/s10801-005-2513-3.

[24] William P. Thurston. Conway's tiling groups. *American Mathematical Monthly*, 97(8): 757–773, 1990.

[25] Panupong Vichitkunakorn. Solutions to the T-Systems with Principal Coefficients. *The Electronic Journal of Combinatorics*, #P2.44, 2016. doi:10.37236/5698

[26] Sicong Zhang. Cluster Variables and Perfect Matchings of Subgraphs of the dP_3 Lattice. arXiv:1511.06055, 2015.

A Minimal matching examples

In this appendix, we present examples of the minimal matching of variant Aztec Castles. In constructing the four sectors, the straight lines are drawn in red, the staircases in purple, and the zero lines in blue.

Region 1: $k \geqslant 1$ and $k-1 < i, j$. This is the top right white region in Figure 11.

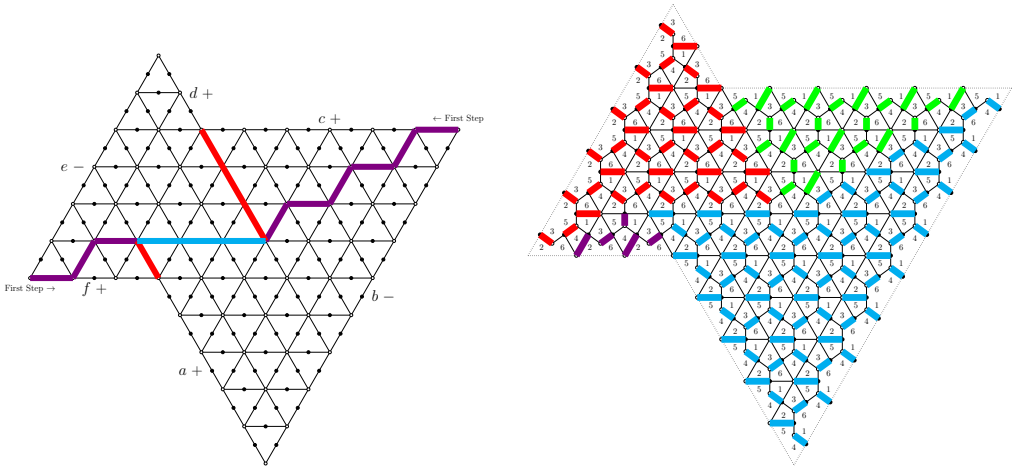

(a) Four sectors (b) Minimal matching

Figure 23: Four sectors and minimal matching of Aztec Castle $\mathcal{C}_{4,3,2}$

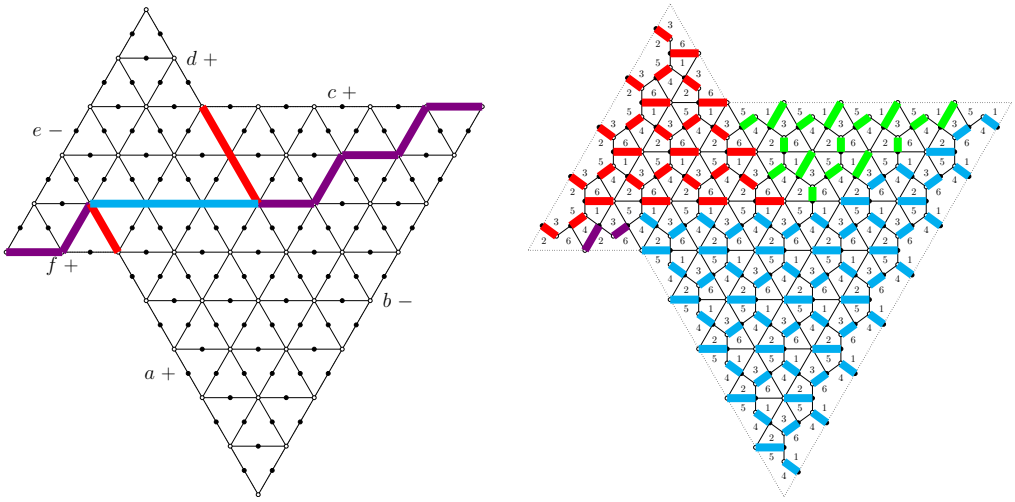

(a) Four sectors (b) Minimal matching

Figure 24: Four sectors and minimal matching of Aztec Castle $\mathcal{C}_{5,3,2}$

Region 2: $k \geqslant 1$ and $-k < i < k-1 < j, i+j$. This is the top middle pink region in Figure 11.

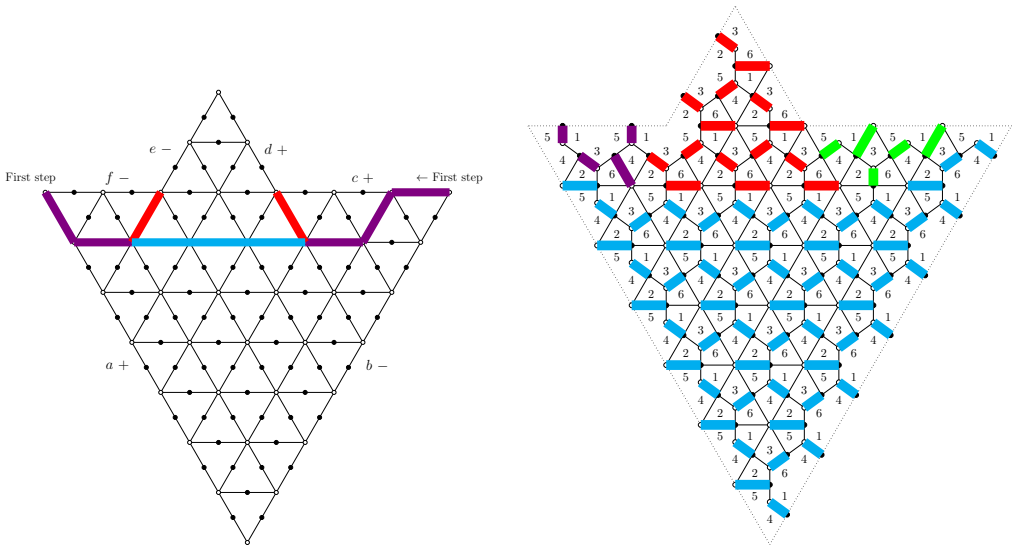

(a) Four sectors (b) Minimal matching

Figure 25: Four sectors and minimal matching of Aztec Castle $\mathcal{C}_{0,4,3}$

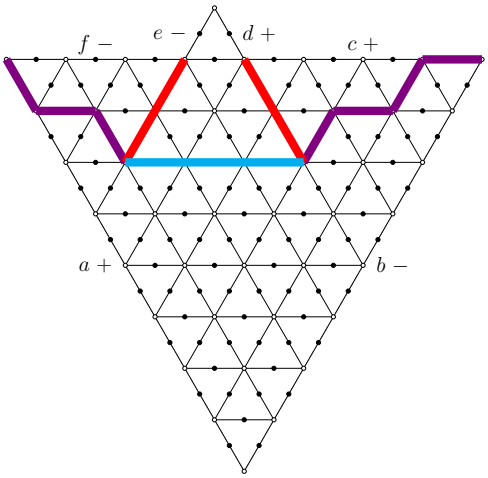

(a) Four sectors

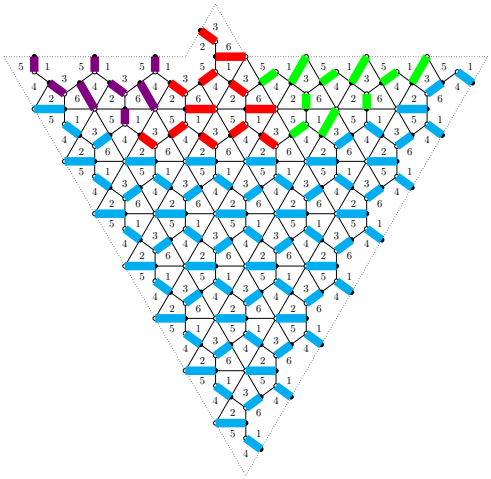

(b) Minimal matching

Figure 26: Four sectors and minimal matching of Aztec Castle $\mathcal{C}_{0,4,4}$

Region 3: $k \geqslant 1$ and $i, j < k-1 < i+j$. This is the blue region in the first quadrant in Figure 11.

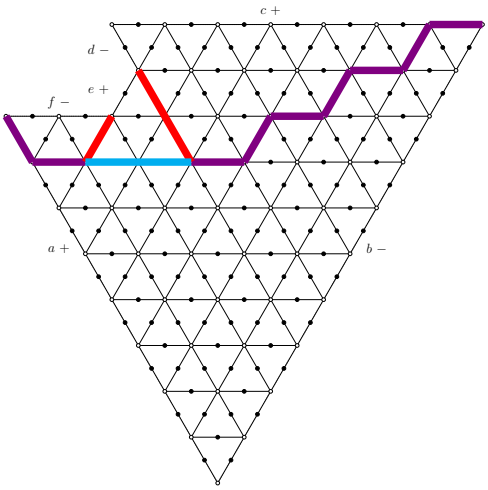

(a) Four sectors

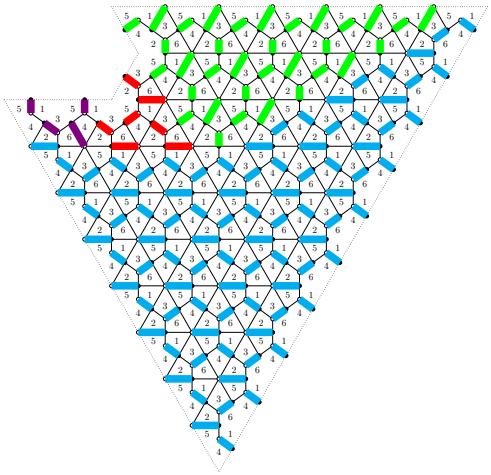

(b) Minimal matching

Figure 27: Four sectors and minimal matching of Aztec Castle $\mathcal{C}_{2,3,5}$

Region 1 ∩ 2: $k \geqslant 1$ and $k-1 = i < j$. This is the intersection of Regions 1 and 2 above.

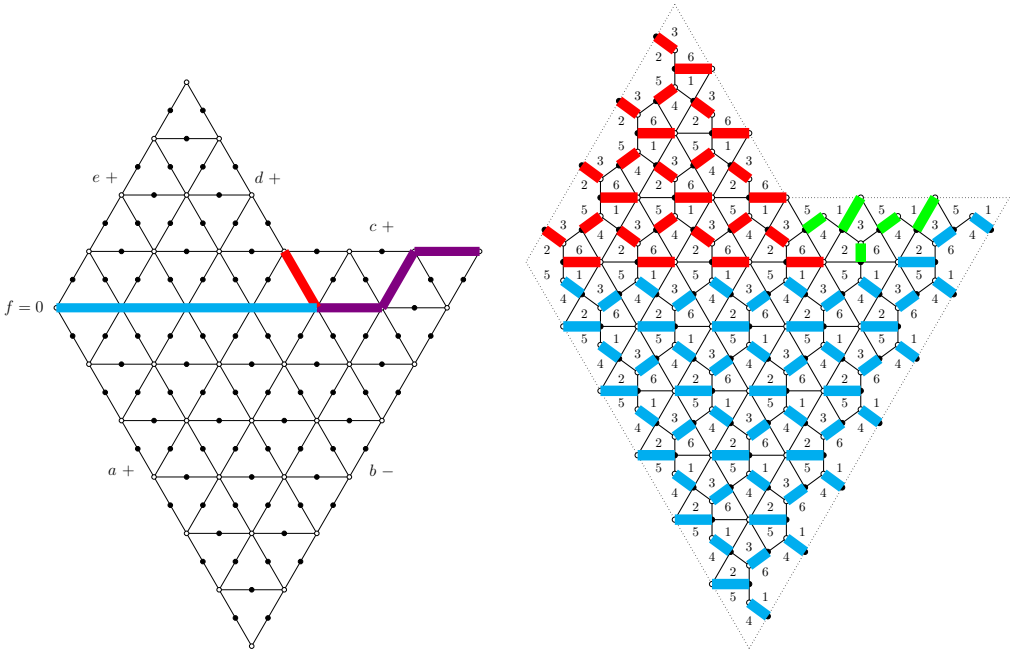

(a) Four sectors (b) Minimal matching

Figure 28: Four sectors and minimal matching of Aztec Castle $\mathcal{C}_{1,4,2}$

Region 2 ∩ 3: $k \geqslant 1$ and $0 < i < k-1 = j$. This is the intersection of Regions 2 and 3 above.

Region 1 ∩ 2 ∩ 3: $k \geqslant 1$ and $i = j = k-1$. This is the point where Regions 1, 2, and 3, as above, intersect.

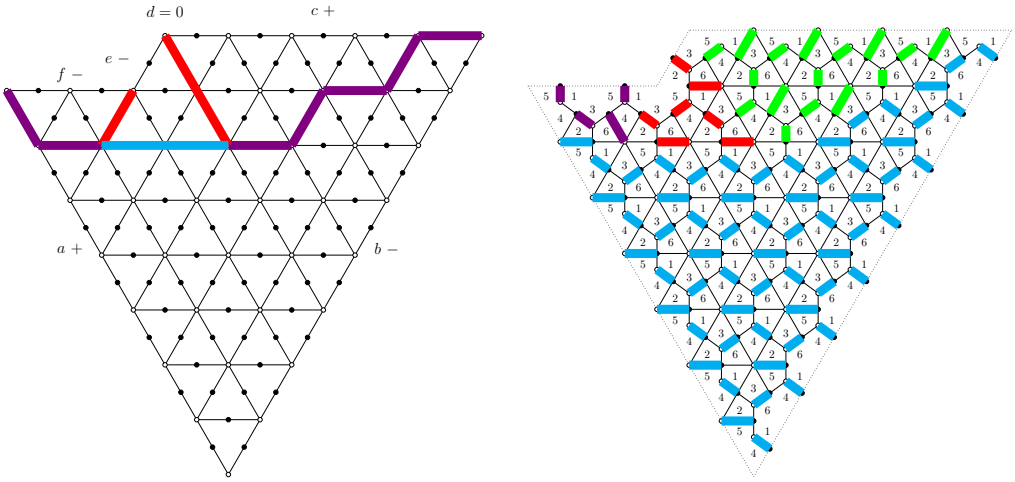

(a) Four sectors (b) Minimal matching

Figure 29: Four sectors and minimal matching of Aztec Castle $\mathcal{C}_{1,3,4}$

B Aztec Dragons

A special family of Aztec Castles is the family of Aztec Dragons, which are Aztec Castles with $i \in \{-1, 0\}, k \in \{0, 1\}$, and $j \geqslant 0$. The weights of Aztec Dragons are the cluster variables of the dP3 quiver after mutations $\tau_1\tau_2\tau_3\tau_1\tau_2\tau_3\ldots$ [26]. Specifically, the four types of Aztec Dragons are

- $D_n = \mathcal{C}_{0,n,1}$,
- $D'_n = \mathcal{C}_{0,n,0}$,
- $D_{n+1/2} = \mathcal{C}_{-1,n+1,0}$, and
- $D'_{n+1/2} = \mathcal{C}_{-1,n+1,1}$.

Note that D_n lies in Region $1 \cap 2$ in Appendix A. D'_n also lies in the same region but with $k \leqslant 0$. $D'_{n+1/2}$ lies in the intersection of Region 2 and 1' in Section 3.2, and $D_{n+1/2}$ lies in the same region but with $k \leqslant 0$. Hence, D'_n is a 180° rotation of D_n, and $D'_{n+1/2}$ is a 180° rotation of $D_{n+1/2}$. In this appendix, we show examples of minimal matchings of Aztec Dragons of the four types.

Type 1: D_n. This is an example of a graph from Region $1 \cap 2$ with $f = 0$. Moreover, side c always has length $i + k = 1$, so the staircase is just a single step which blends into the zero line and the relevant straight lines have length zero. In addition, since the lengths of c and f stay the same, the vertices on the zero line are always covered by the covering of the upper sector.

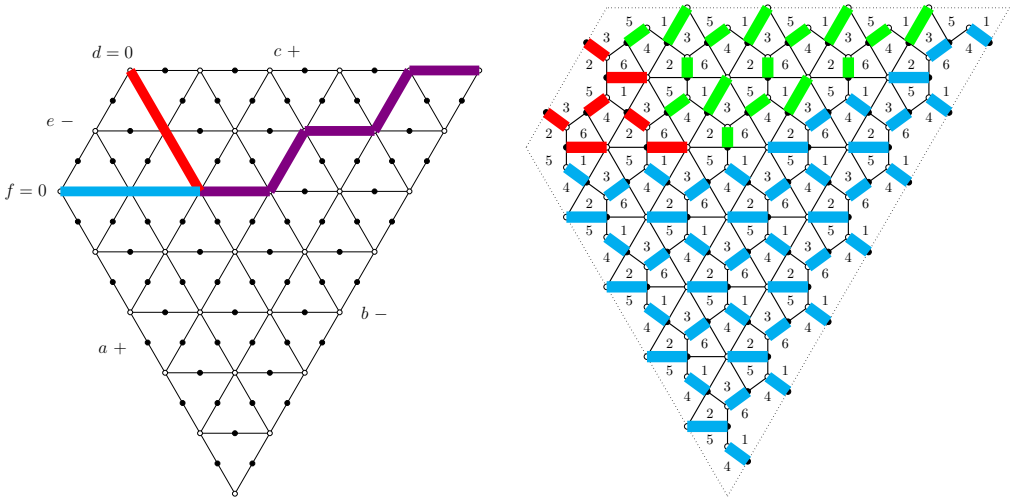

(a) Four sectors (b) Minimal matching

Figure 30: Four sectors and minimal matching of Aztec Castle $\mathcal{C}_{2,2,3}$

Type 2: D'_n. Recall that D'_n is a 180° rotation of D_n, and one can check that Figure 32 is a 180° rotation of Figure 31.

Type 3: $D_{n+1/2}$. Here, we still have $f = 0$ and $c = -1$. Hence, the staircase and straight line both have length 1. Again, since the lengths of c and f stay the same, the vertices on the zero line are always covered by the covering of the upper sector.

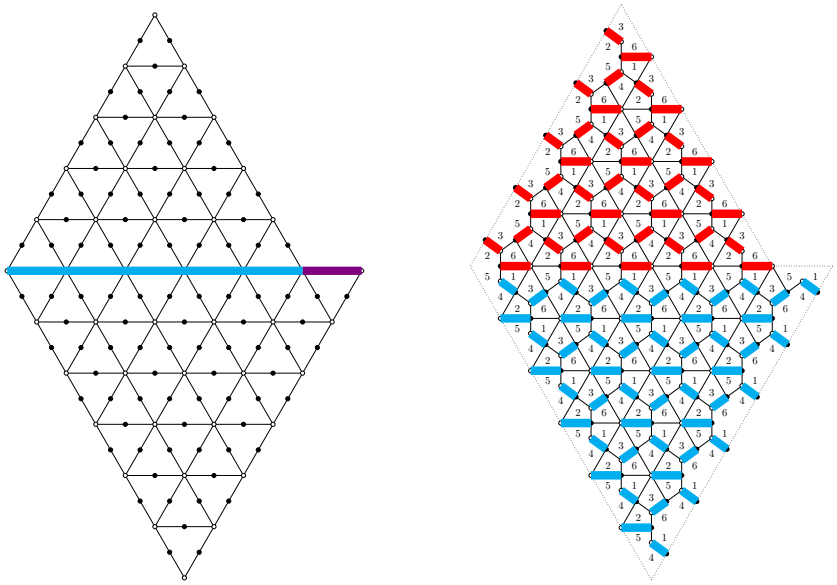

(a) Four sectors (b) Minimal matching

Figure 31: Two sectors and minimal matching of Aztec Dragon $D_5 = \mathcal{C}_{0,5,1}$

Type 4: $D'_{n+1/2}$. Recall that $D'_{n+1/2}$ is a 180° rotation of $D_{n+1/2}$, and one can check that Figure 34 is a 180° rotation of Figure 33.

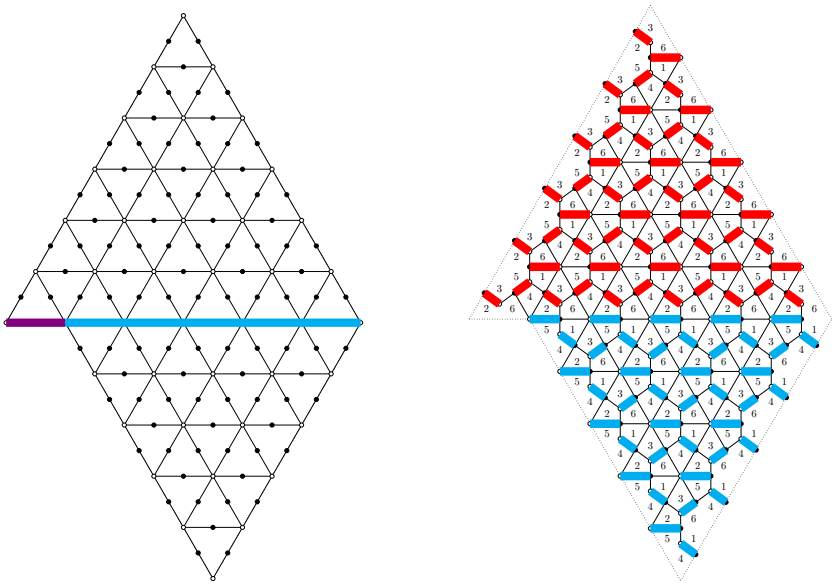

(a) Four sectors (b) Minimal matching

Figure 32: Two sectors and minimal matching of Aztec Dragon $D'_5 = \mathcal{C}_{0,5,0}$

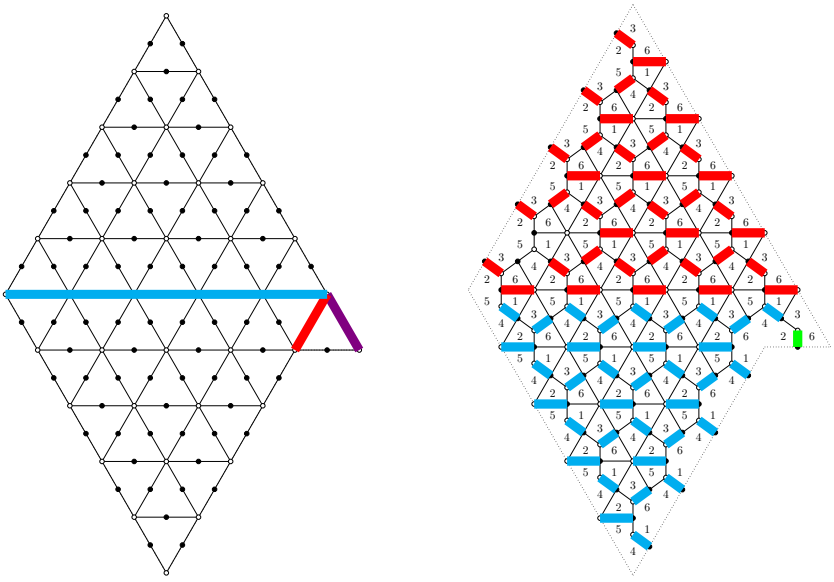

(a) Four sectors (b) Minimal matching

Figure 33: Three sectors and minimal matching of Aztec Dragon $D_{4+1/2} = \mathcal{C}_{-1,5,0}$

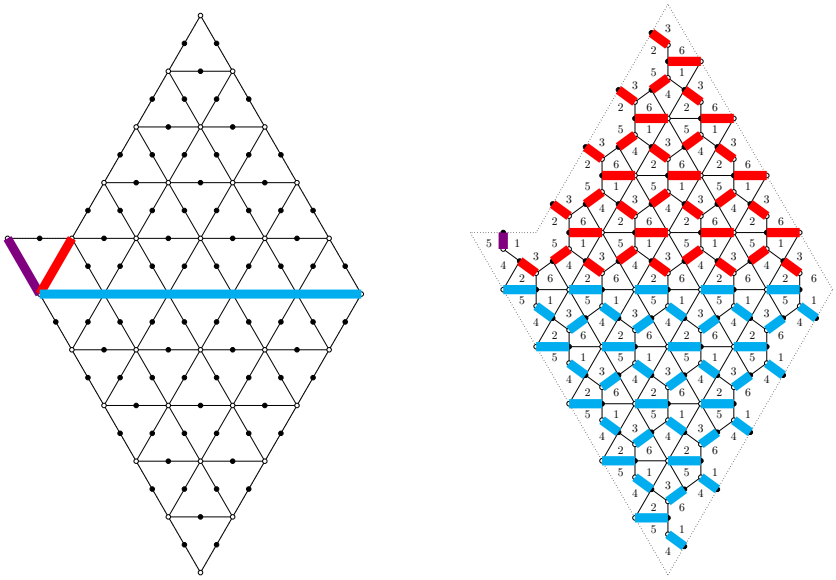

(a) Four sectors (b) Minimal matching

Figure 34: Three sectors and minimal matching of Aztec Dragon $D'_{4+1/2} = \mathcal{C}_{-1,5,1}$